

Polarization states of four-dimensional systems based on biphotons

Yu. I. Bogdanov

Institute of Physics and Technology, Russian Academy of Sciences, 117218 Moscow, Russia

E. V. Moreva*

Moscow Engineering Physics Institute (State University), 115409 Moscow, Russia

G. A. Maslennikov

Department of Physics, National University of Singapore, Singapore, 117542 Singapore

R. F. Galeev, S. S. Straupe, and S. P. Kulik

Faculty of Physics, Moscow State University, 119992 Moscow, Russia

(Received 17 February 2006; published 9 June 2006)

We discuss the concept of polarization states of four-dimensional quantum systems based on the frequency nondegenerate biphoton field. Several quantum tomography protocols were developed and implemented for the measurement of an arbitrary state of ququart. A simple method that does not rely on the interferometric technique is used to generate and measure the sequence of states that can be used for quantum communication purposes.

DOI: [10.1103/PhysRevA.73.063810](https://doi.org/10.1103/PhysRevA.73.063810)

PACS number(s): 42.50.Dv, 03.67.-a

I. INTRODUCTION

Recently multi-dimensional quantum systems (quantum dits, or qudits) attracted much attention in context of quantum information and communication. It is partially caused by fundamental aspects of quantum theory since the usage of qudits allows one to violate Bell-type inequalities longer than with two-dimensional systems (qubits) [1]. Much interest in qudits also comes from their possible usage in the applied quantum key distribution (QKD). Multilevel systems are proved to be more robust against noise in the transmission channel, although measurement and preparation procedures of such systems seem to be much more technically complicated than in the case of qubits. Different aspects of the security of qudit-based QKD protocols have been analyzed [2] including those where the reduced set of bases [3] is used. Lately a proof-of-principle realization of a QKD protocol with qudits [4] and with entangled qutrits ($D=3$, where D is the dimensionality of the Hilbert space) [5] have been demonstrated. For the last several years elegant experiments were performed in which different kinds of optical qudits were introduced. Most of them are based on the states of light emitted via spontaneous parametric down-conversion (SPDC). There are qudits obtained using spatial degrees of freedom: With either single photons [4] or twin photons [6]; orbital angular momentum of photons [7]; time-bin technique [8]; multi-arm interferometers [9]; postselection of polarization qutrits from four-photon states [10]; and polarization states of single-mode biphotons [11].

Although several ways of qudit state preparation have recently been introduced, it seems that until now, there has been only one experiment, demonstrating the complete control over a multilevel state during the preparation stage

within one setup. In this experiment an arbitrary polarization qutrit state (pure or mixed) was generated, exploiting the properties of the single-mode biphoton field [11,12]. However, this method does not allow us to create entangled qutrits. Another disadvantage of using polarization qutrits rises from the fundamental impossibility to switch between arbitrary qutrit states using $SU(2)$ optical elements, like retardation plates, rotators, etc. Meanwhile it is these transformations that would be extremely useful for quantum communication purposes.

In this paper we present the results of the experimental preparation and measurement carried out with polarization based ququarts or quantum systems with dimensionality $D=4$. The paper is organized as follows. In Sec. II we discuss the main properties of ququarts that are generated using the polarization state of the two-photon (biphoton) field. Such operational notions as the coherency matrix and the polarization degree are introduced. The criterion of separability for qubits forming ququarts is discussed as well. Section III describes different experimental techniques of the biphoton-based ququarts preparation and measurement. In Sec. IV we consider a specific set of ququarts which can be used for the practical quantum key distribution.

II. POLARIZATION QUQUARTS AND THEIR PROPERTIES

A. Polarization states of the biphoton field

The biphoton field generated via the spontaneous parametric down-conversion process is represented by a coherent mixture of two-photon Fock states and the vacuum state [13]:

$$\Psi = |\text{vac}\rangle + \frac{1}{2} \sum_{\vec{k}_i, \vec{k}_s} F_{\vec{k}_i, \vec{k}_s} |\vec{1}_{\vec{k}_i}, \vec{1}_{\vec{k}_s}\rangle, \quad (1)$$

where $|\vec{1}_{\vec{k}_i}, \vec{1}_{\vec{k}_s}\rangle$ describes the state with one (idler) photon in the mode \vec{k}_i and one (signal) photon in the mode \vec{k}_s . Since

*Electronic address: ekaterina.moreva@gmail.com

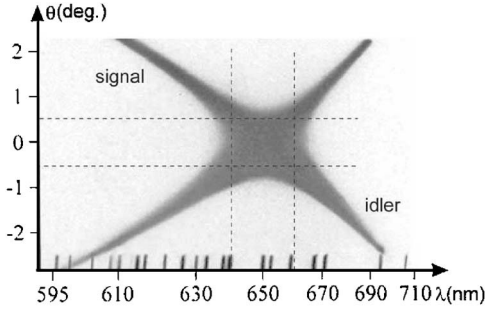


FIG. 1. Photograph of lithium iodate crystal (LiIO_3) frequency-angular spectrum taken with the helium cadmium laser pump operated at 325 nm. The angle between the optical axis of the crystal and the laser pump is 59.22° . Dashed lines select the part of the spectrum (frequency degenerate, collinear regime of SPDC) that contributes to biphoton-based qutrits. Vertical lines at the bottom belong to the spectrum of neon gas which serves as a frequency reference.

squared modulus of the coefficient $F_{\vec{k}_i, \vec{k}_s}^{\vec{r}}$ gives the probability to register two photons in modes k_i and k_s , this quantity is called the biphoton amplitude [14]. The pure polarization state of the down-converted light field, which is often referred as the two-photon field (or biphotons), can be written as follows:

$$|\Psi\rangle = c_1|2_H, 0_V\rangle + c_2|1_H, 1_V\rangle + c_3|1_V, 1_H\rangle + c_4|0_H, 2_V\rangle. \quad (2)$$

Here $c_i = |c_i| e^{i\phi_i}$, $\sum_{i=1}^4 |c_i|^2 = 1$ are complex probability amplitudes. The first (n) and second (m) symbols place in kets correspond to the number of photons with the definite (either horizontal H or vertical V) polarization, the total photon number $m+n=2$. If down-converted photons have equal frequency and momentum, then a ququart state (2) converts to a qutrit state, i.e., middle terms in (2) become indistinguishable: $\vec{k}_s \approx \vec{k}_i$, $\omega_s \approx \omega_i$ and $\omega_s + \omega_i = \omega_p$, where ω_p is the laser pump frequency. In this case any arbitrary pure polarization state of the biphoton field that can be expressed in terms of three complex amplitudes c'_1 , c'_2 , and c'_3 has the following form:

$$|c'\rangle = c'_1|2, 0\rangle + c'_2|1, 1\rangle + c'_3|0, 2\rangle, \quad (3)$$

with $c'_i = |c'_i| \exp\{i\phi_i\}$, $\sum_{i=1}^3 |c'_i|^2 = 1$. The vector $|c'\rangle = (c'_1, c'_2, c'_3)$ represents a three-state system or a qutrit. In Fig. 1 we show a photo of the two-dimensional SPDC spectrum taken in wavelength-angle coordinates. By the convention the left-and-upper side in respect with doubled pump wavelength belongs to the “signal” range whereas the right-and-down side belongs to the “idler” one. The dashed lines limit the central part of the spectrum, which corresponds to the frequency-degenerate and collinear regime when photons forming the biphoton have approximately the same wavelengths and propagate along the pump direction. During the experiment, in order to select this part of the spectrum that corresponds to qutrit states, a set of pinholes and/or narrow-band filters is typically used.

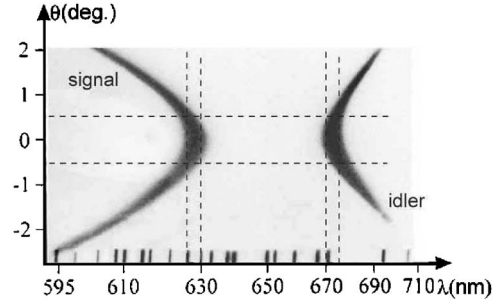


FIG. 2. Nondegenerate regime of SPDC. The angle between the crystal optical axis and the laser pump is 58.97° . Dashed lines select the part of the spectrum contributed to ququarts.

In order to distinguish between the middle terms in (2) one must induce the distinguishability between down-converted photons either in frequency or momentum or detection time. In experiments described in this paper we used the collinear, frequency nondegenerate regime of SPDC so twin photons that form a biphoton had different frequencies and propagated along the same (pump) direction. The two-dimensional SPDC spectrum that describes this situation is shown in Fig. 2. In order to obtain this spectrum it is sufficient to tilt slightly the crystal by a small angle from the orientation that is used for the frequency-degenerate regime. Two dashed rectangles indicate the angular-frequency ranges of the spectrum contributing to ququarts.

The state (2) can be thus rewritten in the form:

$$|\Psi\rangle = c_1|H_1, H_2\rangle + c_2|H_1, V_2\rangle + c_3|V_1, H_2\rangle + c_4|V_1, V_2\rangle. \quad (4)$$

Here $|H_{1(2)}\rangle \equiv a_{1(2)}^\dagger |\text{vac}\rangle$, $|V_{1(2)}\rangle \equiv b_{1(2)}^\dagger |\text{vac}\rangle$, where $a_{1(2)}^\dagger$, $b_{1(2)}^\dagger$ are the creation operators of down-converted photons with central wavelength $\lambda_1(\lambda_2)$ in the horizontal and vertical polarization mode. The alternative way of representing a ququart would be to introduce the distinguishability between spatial modes, while keeping the same central wavelengths of photons: $\vec{k}_s \neq \vec{k}_i$, $\omega_s \approx \omega_i$. The detailed description of polarization properties of such a state of two qubits has been done by James and co-authors [15]. The case of ququart with two frequency modes attracts much attention because for some types of the tasks it is convenient to operate with states in the single spatial mode.

B. Is ququart a separable or entangled state of two qubits?

In general, the state (4) cannot be written as a direct product of polarization states of two photons:

$$|\Psi_1\rangle \otimes |\Psi_2\rangle = (p_1|H_1\rangle + q_1|V_1\rangle) \otimes (p_2|H_2\rangle + q_2|V_2\rangle). \quad (5)$$

That is why it is useful to write down the condition when (4) becomes a separable state. The reduced density matrix of the subsystem (second photon) can be found by tracing the joint state over all states of the first photon:

$$\rho_2 = Sp_1(|\Psi\rangle\langle\Psi|) = \begin{pmatrix} |c_1|^2 + |c_3|^2 & c_1c_2^* + c_3c_4^* \\ c_2c_1^* + c_4c_3^* & |c_2|^2 + |c_4|^2 \end{pmatrix}. \quad (6)$$

It is straightforward to show that the eigenvalues of (6) become $\lambda_{1,2}=0, 1$ and also the entropy of each subsystem drops to zero if

$$c_1c_1^*c_4c_4^* + c_3c_3^*c_2c_2^* - c_2c_1^*c_3c_4^* - c_4c_3^*c_1c_2^* = |c_1c_4 - c_2c_3|^2 = 0. \quad (7)$$

Thus, if $c_1c_4=c_2c_3$ holds, the state (4) can be factorized by definite states of each qubit $|\Psi_1\rangle, |\Psi_2\rangle$ and vice versa. In other words, (7) plays the role of criterion for the biphoton-based polarization ququart to be a separable state of a couple of polarization qubits belonging to two different modes. Subindexes in (4) label either frequency or spatial modes.

As an example, we show different ququart product states that can be generated from a single nonlinear crystal via SPDC:

$$\begin{aligned} \text{type I: } |H_1H_2\rangle &= \begin{pmatrix} 1 \\ 0 \\ 0 \\ 0 \end{pmatrix}, & |V_1V_2\rangle &= \begin{pmatrix} 0 \\ 0 \\ 0 \\ 1 \end{pmatrix}, \\ \text{type II: } |V_1H_2\rangle &= \begin{pmatrix} 0 \\ 0 \\ 1 \\ 0 \end{pmatrix}, & |H_1V_2\rangle &= \begin{pmatrix} 0 \\ 1 \\ 0 \\ 0 \end{pmatrix}, \end{aligned} \quad (8)$$

and maximally entangled Bell states (it requires multiple crystals in one setup):

$$|\Psi^\pm\rangle = \begin{pmatrix} 0 \\ \frac{1}{\sqrt{2}} \\ \pm \frac{1}{\sqrt{2}} \\ 0 \end{pmatrix}, \quad |\Phi^\pm\rangle = \begin{pmatrix} \frac{1}{\sqrt{2}} \\ 0 \\ 0 \\ \pm \frac{1}{\sqrt{2}} \end{pmatrix}. \quad (9)$$

At the end of this section we would like to mention that in the general case, a pure polarization ququart state cannot be mapped as a pair of points on the Poincaré sphere as it occurs for biphoton-based qutrits [16,17]. It is so because the state (4) cannot be factorized in general. However, if criterion (7) is satisfied, the subset of separable qubit states admits its visual representation on the Poincaré sphere.

C. Second-order of the field: Stokes parameters

Polarization properties of a pure state (4) can be described by Stokes parameters which are defined as mean values of Stokes operators averaged over the state (4). Although the description of the light polarization can be introduced only for the quasimonochromatic plane waves, it is possible to use P -quasispin formalism [18] to describe the polarization of arbitrary quantum beams with n modes, frequency or spatial.

For the two-frequency and single-spatial mode field, the Stokes parameters will contain time and frequency dependent terms $\exp[i(\omega_j - \omega_k)t]$ that describe “beats” of frequency modes and do not describe the biphoton light polarization. However, these terms vanish if one considers the finite detection time that allows one to classically average these “beatings.” So in the case of the two-frequency biphoton field, the Stokes operators are given by the sum of corresponding operators in two frequency modes.

$$\begin{aligned} \langle S_0 \rangle &= \langle a_1^\dagger a_1 + a_2^\dagger a_2 + b_1^\dagger b_1 + b_2^\dagger b_2 \rangle \equiv \langle S_0^{(1)} \rangle + \langle S_0^{(2)} \rangle = 2; \\ \langle S_1 \rangle &= \langle a_1^\dagger a_1 + a_2^\dagger a_2 - b_1^\dagger b_1 - b_2^\dagger b_2 \rangle \\ &\equiv \langle S_1^{(1)} \rangle + \langle S_1^{(2)} \rangle = 2(|c_1|^2 - |c_4|^2); \\ \langle S_2 \rangle &= \langle a_1^\dagger b_1 + a_2^\dagger b_2 + b_1^\dagger a_1 + b_2^\dagger a_2 \rangle \\ &\equiv \langle S_2^{(1)} \rangle + \langle S_2^{(2)} \rangle = 2 \operatorname{Re}(c_1^*(c_2 + c_3) + c_4(c_2^* + c_3^*)); \\ \langle S_3 \rangle &= \langle a_1^\dagger b_1 + a_2^\dagger b_2 - b_1^\dagger a_1 - b_2^\dagger a_2 \rangle \\ &\equiv \langle S_3^{(1)} \rangle + \langle S_3^{(2)} \rangle = 2 \operatorname{Im}(c_1^*(c_2 + c_3) + c_4(c_2^* + c_3^*)). \end{aligned} \quad (10)$$

The same definition applies to the second wavelength λ_2 and we take into account that these operators do not commute for different frequency modes.

D. Fourth-order of the field: Coherency matrix

Polarization properties of biphoton-based ququarts are determined completely by the coherency matrix. It is a matrix consisting of ten fourth-order moments of the electromagnetic field. An ordered set of such moments can be obtained using the direct product of 2×2 -coherency matrices for both polarization qubits forming the biphoton:

$$K_4 \equiv (K_2)_1 \otimes (K_2)_2 = \begin{pmatrix} A & E & F & G \\ E^* & B & I & K \\ F^* & I^* & C & L \\ G^* & K^* & L^* & D \end{pmatrix}, \quad (11)$$

where $(K_2)_{j,2}$ are 2×2 -coherency matrices for single photons with different frequencies marked by indices $j=1, 2$:

$$(K_2)_j \equiv \begin{pmatrix} \langle a_j^\dagger a_j \rangle & \langle a_j^\dagger b_j \rangle \\ \langle a_j b_j^\dagger \rangle & \langle b_j^\dagger b_j \rangle \end{pmatrix}. \quad (12)$$

The diagonal elements of (11) are formed by moments, which characterize the intensity correlation in two polarization modes H and V :

$$\begin{aligned} A &\equiv \langle a_1^\dagger a_2^\dagger a_1 a_2 \rangle = |c_1|^2, & B &\equiv \langle a_1^\dagger b_2^\dagger a_1 b_2 \rangle = |c_2|^2, \\ C &\equiv \langle b_1^\dagger a_2^\dagger b_1 a_2 \rangle = |c_3|^2, & D &\equiv \langle b_1^\dagger b_2^\dagger b_1 b_2 \rangle = |c_4|^2. \end{aligned} \quad (13)$$

Nondiagonal moments are complex:

$$\begin{aligned} E &\equiv \langle a_1^\dagger a_2^\dagger a_1 b_2 \rangle = c_1^* c_2, & F &\equiv \langle a_1^\dagger a_2^\dagger b_1 a_2 \rangle = c_1^* c_3, \\ G &\equiv \langle a_1^\dagger a_2^\dagger b_1 b_2 \rangle = c_1^* c_4, & I &\equiv \langle a_1^\dagger b_2^\dagger b_1 a_2 \rangle = c_2^* c_3, \\ K &\equiv \langle a_1^\dagger b_2^\dagger b_1 b_2 \rangle = c_2^* c_4, & L &\equiv \langle b_1^\dagger a_2^\dagger b_1 b_2 \rangle = c_3^* c_4. \end{aligned} \quad (14)$$

The averaging in (13) and (14) is taken over the state (4). The polarization (reduced) density matrix of ququart state coincides with coherency matrix K_4 .

E. Polarization degree and transformations of ququarts

The polarization degree is given by

$$P = \frac{\sqrt{\sum_{k=1}^3 \langle S_k \rangle^2}}{\langle S_0 \rangle} = \frac{\sqrt{\sum_{k=1}^3 \langle S_k^{(1)} + S_k^{(2)} \rangle^2}}{\langle S_0^{(1)} + S_0^{(2)} \rangle}. \quad (15)$$

This definition of polarization degree is just generalization of the commonly used classical one. It differs from the definition suggested in [19], where it serves as a witness of the state purity. In the case of polarization qutrit states [11,12], the polarization degree is

$$P_3 = \sqrt{|c'_1|^2 - |c'_3|^2 + 2|c'_1 c'_2 + c'_2 c'_3|^2} \quad (16)$$

with $c'_1 = c_1, \sqrt{2}c'_2 = c_2 = c_3, c'_3 = c_4$. The polarization degree of a qutrit state is invariant under unitary polarization transformations, which is reasonably straightforward [20]. Indeed it is impossible to prepare all demanded pure states that can be used, for example, in QKD protocols unless one uses interferometric schemes with several nonlinear crystals [11], or introduces losses. In particular, there is no way to transform the basic qutrit state $|\Psi'_4\rangle = |V, V\rangle$ with $P=1$ into orthogonal state $|\Psi'_2\rangle = |H, V\rangle$ with $P=0$ using SU(2) transformations (retardation plates, etc.) [21]. However, in the case of polarization ququarts, this quantity is no longer invariant. Indeed, the polarization degree (15) can be rewritten as

$$P_4 = \frac{\sqrt{\sum_{j=1}^2 (Tr^2(K_2)_j - 2 \det(K_2)_j) + 2 \sum_{k=1}^3 \langle S_k^{(1)} S_k^{(2)} \rangle}}{\sum_{j=1}^2 Tr(K_2)_j}. \quad (17)$$

In (17) we used trivial links between coherency matrices and Stokes parameters [23].

Both the expression in the round brackets and the denominator are invariant under unitary transformations as well as the denominator. The second term under the square root in the numerator can be expanded in terms of fourth-order moments:

$$\sum_{k=1}^3 \langle S_k^{(1)} S_k^{(2)} \rangle = \{Tr K_4 - 2(\text{Re } I + B + C)\}. \quad (18)$$

Since unitary transformations keep the number of photons, then $Tr K_4$ is invariant. At the same time it is easy to prove that the combination of moments $\text{Re } I + B + C$ is not invariant, so the whole expression (17) changes under SU(2) transformations. As a consequence, the polarization degree changes by applying local unitary transformations in each frequency mode. This can be done in an experiment by using dichroic polarization transformers, which act separately on

the photons with different frequencies. For example, to perform the following transformation

$$|\Psi_4\rangle = |V_{\lambda_1}, V_{\lambda_2}\rangle \Rightarrow |\Psi_2\rangle = |H_{\lambda_1}, V_{\lambda_2}\rangle, \quad (19)$$

one needs to use the retardation plate that serves as a half-wave plate at λ_1 and as a wave plate at λ_2 . In the general case when ququart is not a product state of two qubits the transformation matrix \hat{G} :

$$|\Psi\rangle^{out} = \hat{G}|\Psi\rangle^{in} \quad (20)$$

can be found simply in Heizenberg representation. We use the equivalent representation of (4) using creation and annihilation operators:

$$|\Psi\rangle^{in} = [c_1 a_1^\dagger a_2^\dagger + c_2 a_1^\dagger b_2^\dagger + c_3 b_1^\dagger a_2^\dagger + c_4 b_1^\dagger b_2^\dagger] |\text{vac}\rangle. \quad (21)$$

SU(2) transformation between input a_j, b_j and output a'_j, b'_j operators is given by:

$$\begin{aligned} a'_j &= t_j a_j + r_j b_j, \\ b'_j &= -r_j^* a_j + t_j^* b_j, \end{aligned} \quad (22)$$

where

$$t_j = \cos \delta_j + i \sin \delta_j \cos 2\alpha_j,$$

$$r_j = i \sin \delta_j \sin 2\alpha_j, \quad \delta_j = \pi(n_{o_j} - n_{e_j})h/\lambda_j. \quad (23)$$

Here t_j and r_j are the amplitude transmission and reflection coefficients of the wave plate, δ_j is its optical thickness, h is the geometrical thickness, α_j is the orientation angle between the optical axis of the wave plate and vertical direction. Lower indices $j=1, 2$ label the frequency modes of photons. Substituting (22) into (21) one can immediately find that the unitary transformation on state (4) is given by 4×4 matrix which is obtained by a direct product of two 2×2 matrices describing the transformation performed on each photon [20]:

$$\begin{aligned} \hat{G} &\equiv \begin{pmatrix} t_1 t_2 & t_1 r_2 & r_1 t_2 & r_1 r_2 \\ -t_1 r_2^* & t_1 t_2^* & -r_1 r_2^* & r_1 t_2^* \\ -r_1^* t_2 & -r_1^* r_2 & t_1^* t_2 & t_1^* r_2 \\ r_1^* r_2^* & -r_1^* t_2^* & -t_1^* r_2^* & t_1^* t_2^* \end{pmatrix} \\ &= \begin{pmatrix} t_1 & r_1 \\ -r_1^* & t_1^* \end{pmatrix} \otimes \begin{pmatrix} t_2 & r_2 \\ -r_2^* & t_2^* \end{pmatrix}. \end{aligned} \quad (24)$$

It is important to note that the optical thickness δ depends on the wavelength, so parameters t and r which determine the result of transformation differ for photons forming the biphoton-based ququart. Thus for the ququart transformation (without taking a nonessential phase term into account) considered above in (19), matrix G becomes

$$\hat{g} \equiv \begin{pmatrix} 0 & 0 & 1 & 0 \\ 0 & 0 & 0 & 1 \\ 1 & 0 & 0 & 0 \\ 0 & 1 & 0 & 0 \end{pmatrix}. \quad (25)$$

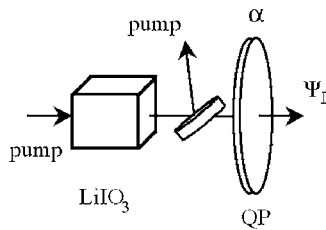


FIG. 3. Preparation of states Ψ_I . A nonlinear crystal generates one of the basic ququart state(s) via type-I SPDC. Then the state is transformed by the wave plate QP with the parameters depending on its orientation angle α .

The same dichroic plate performs unitary transformations between polarization Bell states: $g|\Phi^\pm\rangle=|\Psi^\pm\rangle$, and $g|\Psi^\pm\rangle=|\Phi^\pm\rangle$, where $|\Phi^\pm\rangle$ and $|\Psi^\pm\rangle$ are represented by ququarts with $c_1=\pm c_4=1/\sqrt{2}$ and $c_2=\pm c_3=1/\sqrt{2}$ correspondingly. Similar transformations with frequency nondegenerate biphotons propagating in the single spatial mode have been realized in [22].

III. EXPERIMENTAL IMPLEMENTATION

In this section we describe several methods of ququart state preparation and measurement.

A. Preparation

In general to prepare an arbitrary ququart state (4) it is necessary to use four nonlinear crystals arranged in such a way that each crystal emits coherently one basic state in the same direction. But in special cases, a reduced set of crystals is sufficient to generate the specific ququart states that can be used in practice. In the experiments described below we used the following methods to generate a subset of ququart states.

1. Separable states

If a nonlinear crystal generates one of the basic states, (8) then applying the transformation (24) one can get a subset of ququarts which are the product states of polarization qubit pairs (Fig. 3). We used the basic state $|V_1V_2\rangle$, so the states generated by this method have the following structure:

$$|\Psi_I(\alpha)\rangle = \begin{pmatrix} r_1 r_2 \\ r_1 t_2^* \\ t_1^* r_2 \\ t_1^* t_2^* \end{pmatrix}. \quad (26)$$

Since coefficients r_j and t_j depend on the orientation angle α_j , there is a simple way to transform the state by rotating the retardant plate. As we will show below, a use of a single crystal allows one to prepare the whole subset of ququarts which can be used for the quantum key distribution.

2. Entangled states

To prepare the ququarts with $c_1 c_4 \neq c_2 c_3$ it is sufficient to use two crystals as it was done when frequency nondegenerate Bell states have been generated [24] (Fig. 4).

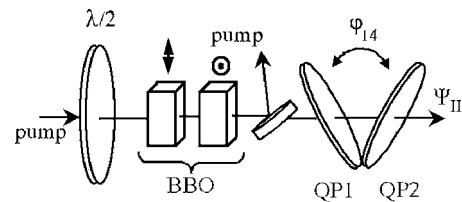


FIG. 4. Preparation of states Ψ_{II} . Two nonlinear crystals generate a pair of the basic ququart states via type-I SPDC. The relative phase between states φ_{14} is controlled by two quartz plates QP1, QP2. The basic state amplitudes are controlled with the help of the half-wave plate.

In order to introduce a phase shift φ_{14} between horizontally and vertically polarized type-I biphotons, two 1 mm quartz plates (QP1,2) that can be rotated along the optical axis were used. By tilting the plates the following family of ququarts were generated:

$$|\Psi_{II}(\phi)\rangle = \begin{pmatrix} |c_1| \\ 0 \\ 0 \\ |c_4|e^{-i\varphi_{14}} \end{pmatrix}, \quad (27)$$

where real amplitudes $|c_1|, |c_4|$ were controlled by the half wave plate inserted into the linearly polarized pump beam. Remarkable interference phenomena with $|\Psi_{II}(\phi)\rangle$ -like states were observed. For example, when the phase of λ_1 -photon is altered, then the modulation with the same wavelength is observed in the coincidence rate, while varying the phase of second photon λ_2 -wavelength modulation is observed [24]. Transformations of frequency nondegenerate Bell states experimentally have been studied in [22]. Another effect related to biphoton-based ququarts that is widely discussed in quantum optics is “hidden polarization.”

B. Measurement

Basically it is necessary to perform D^2 independent measurements for the complete reconstruction of the arbitrary qudit density matrix. So for $D=4$ the total number of measurements is equal to sixteen. Since the only way to measure a biphoton is to register a coincidence of photocounts, we choose the Brown-Twiss scheme supplied with polarization elements to perform projective measurements. A coincidence click that occurs when signals from two detectors fall into the coincidence window is considered a registered event. Since the coincidence click appears at the output with some probability, a statistical treatment of outcomes becomes very important. Another point that we would like to note is that according to Bohr’s complementarity principle, there is no way to measure all moments (13) and (14) at the same time, dealing with a single ququart only. So to perform a complete set of measurements one needs to generate a lot of representatives of a quantum ensemble.

In order to measure the ququarts we developed two protocols.

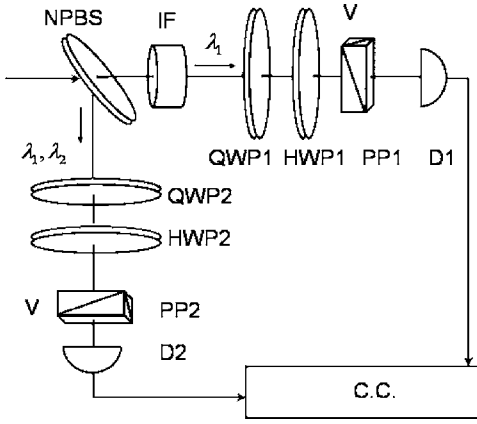


FIG. 5. Measurement block for Protocol 1. Brown-Twiss scheme for measuring the intensity correlation between two polarization modes. After the spatial separation at the nonpolarizing 50/50 beam-splitter (NPBS), signal (λ_2) and idler (λ_1) photons propagate through the quarter- (QWP1,2) and half- HWP1,2 -wave plates, polarizing prisms (PP1,2) placed in both channels. The interference filter centered at λ_1 (IF) placed in the upper arm selects one frequency mode of a ququart. Finally, photons are registered by detectors (D1,2). The coincidence rate at the output of the coincidence circuit (CC) is proportional to the fourth moment in the field $\langle R \rangle$.

1. Protocol 1

The idea of the first method is to split the ququart state $|\Psi_{in}\rangle$ into two frequency modes and to perform transformations independently on each photon from the pair (Fig. 5). Usage of a dichroic beam-splitter allows one to separate frequency modes in space and reduce this protocol to that one developed in [15] for two spatially separated polarization qubits. We called this method “frequency selective” because frequency mode separation is basically applied to the ququart before subjecting it to polarization projective measurements.

The polarization transformations can be done by using polarization filters placed in front of detectors. Each filter consists of a sequence of quarter- and half-wave plates and a polarization prism which transmits vertical polarization. In our experiments we kept the protocol developed in [15] unchanged, although there are many other configurations of polarization filters leading to the matrix K_4 reconstruction. Instead of a dichroic beam-splitter we used a (50/50)% polarization insensitive beam-splitter and a narrow-band filter centered at λ_1 that was put in front of the first detector. In such a way we postselected the desirable events in registered coincidences. Approximately in a quarter of trials, the photons with central wavelength λ_1 forming a biphoton are going to the first detector, while the conjugated ones (with central wavelength λ_2) are going to the second detector. In the remaining cases, the events are not registered because either they do not contribute to coincidences or corresponding photons do not pass through the interference filter.

In Heisenberg representation the polarization transformation for each output port of the dichroic beam-splitter is given by:

$$\begin{pmatrix} a_j^\dagger \\ b_j^\dagger \end{pmatrix} = \begin{pmatrix} 0 & 0 \\ 0 & 1 \end{pmatrix} D_{\lambda_j/2}(\delta_j = \pi/2, \theta) D_{\lambda_j/4}(\delta_j = \pi/4, \chi) \\ \times \begin{pmatrix} \frac{1}{\sqrt{2}} & 0 \\ 0 & \frac{1}{\sqrt{2}} \end{pmatrix} \begin{pmatrix} a_j^\dagger \\ b_j^\dagger \end{pmatrix}. \quad (28)$$

We label different output ports of the beam-splitter which correspond to different wavelengths $\lambda_{1,2}$ with indices $j = 1, 2$. Four 2×2 matrices in the right-hand side of (28) describe the action of the nonpolarizing beam-splitter, $\lambda/4$ -, $\lambda/2$ -plates and vertical polarization prism on the state vector of each photon;

$$D_{\lambda_j/2, \lambda_j/4} = \begin{pmatrix} t_j & r_j \\ -r_j^* & t_j^* \end{pmatrix},$$

where r_j and t_j are the coefficients introduced in Eq. (23), so for a $\lambda_j/4$ -plate ($\delta_j = \pi/4$)

$$t_{\lambda_j/4} = \frac{1}{\sqrt{2}}(1 + i \cos 2\chi_j), \quad r_{\lambda_j/4} = \frac{i}{\sqrt{2}} \sin 2\chi_j \quad (29a)$$

and for a $\lambda_j/2$ -plate ($\delta_j = \pi/2$)

$$t_{\lambda_j/2} = i \cos(2\theta_j), \quad r_{\lambda_j/2} = i \sin(2\theta_j). \quad (29b)$$

Thus, there are four real parameters (two for each channel) that determine polarization transformations. Namely, these parameters are orientation angles for two pairs of wave plates: $\theta_1, \chi_1, \theta_2, \chi_2$. Also we would like to note that there is another parameter that affects strongly the result of polarization transformations. It is a wavelength(s) of down-converted photon(s). For example, varying the frequency spectrum of SPDC by tilting a crystal which generates biphotons, one can significantly change the transformed state (20) using fixed parameters of the wave plates such as geometrical thickness h and its orientation α . This property makes biphoton-based ququarts more controllable than biphoton-based qutrits and allows one to choose convenient regimes for dealing with them.

As it was mentioned above, the registered signal from Brown-Twiss scheme is the coincidence rate of the pulses coming from two detectors D_1 and D_2 . The fourth-order moment of the field that corresponds to a registered coincidence event has the following structure:

$$R_{1,2} \propto \langle b_1^\dagger b_2^\dagger b_1' b_2' \rangle = R(\theta_1, \chi_1, \theta_2, \chi_2). \quad (30)$$

In the most general case this moment contains a linear combination of ten moments (13) and (14) that form matrix K_4 . So the main purpose of the state reconstruction procedure is to extract these moments from the registered coincidence rate for different orientations of the polarization filters in the Brown-Twiss scheme. Let us consider some special examples which give the corresponding lines in the complete protocol introduced below (Table I). The measurement of the first four moments (13) is a trivial procedure. For instance, the third line in Table I corresponds to filtering out the basic state $|\Psi_1 \Psi_2\rangle$. The other three upper lines correspond to the

TABLE I. Protocol 1. Each line contains the orientation of the half- ($\theta_{s,i}$) and quarter- ($\chi_{s,i}$) wave plates in the measurement block. Last two columns show the corresponding moment R_ν and the process amplitude M_ν ($\nu=1, \dots, 16$). Sign “-” in the orientation of the plates for the reflection channel is introduced to compensate π -phase shift occurring after the reflection from the beam-splitter.

ν	Set-up parameters				Moments to be measured	Amplitude of the process
	χ_s	θ_s	χ_i	θ_i	$R_\nu = M_\nu ^2$	M_ν
1.	0	45°	0	-45°	$A/4$	$c_1/2$
2.	0	45°	0	0	$B/4$	$c_2/2$
3.	0	0	0	0	$D/4$	$c_4/2$
4.	0	0	0	-45°	$C/4$	$c_3/2$
5.	0	22.5°	0	-45°	$1/8(A+C+2 \operatorname{Im} F)$	$1/2\sqrt{2}(c_1-ic_3)$
6.	0	22.5°	0	0	$1/8(B+D+2 \operatorname{Im} K)$	$1/2\sqrt{2}(c_2-ic_4)$
7.	45°	22.5°	0	0	$1/8(B+D-2 \operatorname{Re} K)$	$1/2\sqrt{2}(c_2-c_4)$
8.	45°	22.5°	0	-45°	$1/8(A+C-2 \operatorname{Re} F)$	$1/2\sqrt{2}(c_1-c_3)$
9.	45°	22.5°	0	-22.5°	$1/16(A+B+C+D)-1/8(\operatorname{Im} E+\operatorname{Re} F$ $- \operatorname{Im} G+\operatorname{Im} I+\operatorname{Re} K+\operatorname{Im} L)$	$1/4[(c_1-c_3)+i(c_2-c_4)]$
10.	45°	22.5°	-45°	-22.5°	$1/16(A+B+C+D)-1/8(\operatorname{Re} F-\operatorname{Re} E$ $+ \operatorname{Re} G+\operatorname{Re} I+\operatorname{Re} K-\operatorname{Re} L)$	$1/4[c_1+c_2-c_3-c_4]$
11.	0	22.5°	-45°	-22.5°	$1/16(A+B+C+D)+1/8(\operatorname{Im} F+\operatorname{Re} E$ $+ \operatorname{Im} G+\operatorname{Im} I+\operatorname{Re} L+\operatorname{Im} K)$	$1/4[(c_1+c_2)-i(c_3+c_4)]$
12.	0	45°	-45°	-22.5°	$1/8(A+B+2 \operatorname{Re} E)$	$1/2\sqrt{2}(c_1+c_2)$
13.	0	0	-45°	-22.5°	$1/8(C+D+2 \operatorname{Re} L)$	$1/2\sqrt{2}(c_3+c_4)$
14.	0	0	-90°	-22.5°	$1/8(C+D+2 \operatorname{Im} L)$	$1/2\sqrt{2}(c_3-ic_4)$
15.	0	45°	-90°	-22.5°	$1/8(A+B+2 \operatorname{Im} E)$	$1/2\sqrt{2}(c_1-ic_2)$
16.	0	22.5°	-90°	-22.5°	$1/16(A+B+C+D)+1/8(\operatorname{Im} F+\operatorname{Im} E$ $- \operatorname{Re} G+\operatorname{Re} I+\operatorname{Im} L+\operatorname{Im} K)$	$1/4[(c_1-c_4)-i(c_2+c_3)]$

measurements of other basic states $|H_1H_2\rangle$, $|H_1V_2\rangle$, and $|V_1H_2\rangle$. Remaining lines of protocol show the orientations of the wave plates that were used to measure the complex moments (14). For example, in order to measure the real part of moment E , let us set the wave plates in the Brown-Twiss scheme in the following way.

The first channel:

$$\lambda/4: \quad \chi_1 = 0^\circ, \quad D_{\lambda/4} = \frac{1}{\sqrt{2}} \begin{pmatrix} 1+i & 0 \\ 0 & 1-i \end{pmatrix}; \quad (31a)$$

$$\lambda/2: \quad \theta_1 = 45^\circ, \quad D_{\lambda/2} = \begin{pmatrix} 0 & i \\ i & 0 \end{pmatrix}. \quad (31b)$$

The second channel:

$$\lambda/4: \quad \chi_2 = -45^\circ, \quad D_{\lambda/4} = \frac{1}{\sqrt{2}} \begin{pmatrix} 1 & -i \\ -i & 1 \end{pmatrix}; \quad (32a)$$

$$\lambda/2: \quad \theta_2 = -22.5^\circ, \quad D_{\lambda/2} = \frac{1}{\sqrt{2}} \begin{pmatrix} i & -i \\ -i & -i \end{pmatrix}. \quad (32b)$$

Substituting these matrices into Eq. (28) and taking into account the commutation rules for the creation and annihilation operators, it is easy to get the final moment measured in the experiment:

$$R = \langle \Psi | b_1^\dagger b_2^\dagger b_1 b_2 | \Psi \rangle = 1/8(A + C + 2 \operatorname{Re} E).$$

A complete set of projective measurements that is called a tomography protocol is presented in Table I. Each row corresponds to the setting of the wave plates that were used to measure the moment highlighted in the sixth column. The last column corresponds to the amplitude of the process (see below).

Amplitude M_ν of the quantum process describing the passage of down-converted photons through the measurement setup for each configuration of wave plates is determined by the following equation:

$$M_\nu(\delta_1, \theta_k, \delta_2, \varphi) = \frac{1}{2} [a_1 a_2 c_1 + a_1 b_2 c_2 + b_1 a_2 c_3 + b_1 b_2 c_4], \quad (33)$$

where

$$\begin{aligned} a_1 &= -r_{\lambda/2}(\theta_1) t_{\lambda/4}^*(\chi_1) - t_{\lambda/2}(\theta_1) r_{\lambda/4}(\chi_1), \\ a_2 &= -r_{\lambda/2}(\theta_2) t_{\lambda/4}^*(\chi_2) - t_{\lambda/2}(\theta_2) r_{\lambda/4}(\chi_2), \\ b_1 &= -r_{\lambda/2}(\theta_1) r_{\lambda/4}^*(\chi_1) + t_{\lambda/2}(\theta_1) t_{\lambda/4}(\chi_1), \\ b_2 &= -r_{\lambda/2}(\theta_2) r_{\lambda/4}^*(\chi_2) + t_{\lambda/2}(\theta_2) t_{\lambda/4}(\chi_2). \end{aligned} \quad (34)$$

The complete reconstruction of input state $|\Psi^{in}\rangle$ was performed according to the algorithm considered in our previous work [12].

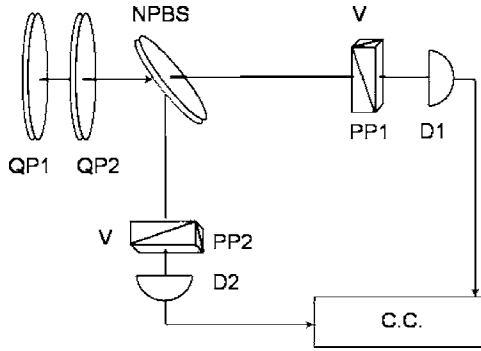


FIG. 6. Measurement block for Protocol 2. After the input state is subjected to the transformations by wave plates (QP1, QP2), the projective measurements selecting vertical polarizations of ququart components are performed.

Concluding this section we would like to stress that if a usual frequency insensitive (broadband) beam-splitter is used and no interference filters are inserted either in front of or behind this beam-splitter, then a “nonselective” method of ququart measurement is possible. In this case one does not need to use the interference filter to select the wavelength in each channel of Brown-Twiss scheme. In other words, each detector is allowed to register photons with different frequencies and the fourth moment of the field that is measured in the experiment is given by

$$R_{1,2} \propto \langle (b'_1 + b'_2)_{\text{Detector2}}^\dagger (b'_1 + b'_2)_{\text{Detector1}} \rangle \quad (35)$$

instead of (30). In a nonselective method the expression connecting observable value $R_{1,2}$ with components of coherence matrix (13) and (14) is too cumbersome and it is not reasonable to use it for the state reconstruction. However, in special cases we applied a nonselective method to the ququart reconstruction procedure and developed the special protocol, which is introduced in the next section.

2. Protocol 2

In the second protocol the whole ququart state (2) is subjected to the linear transformations that are done by a set of the retardation plates [25]. Then projective measurements are applied to state $|\Psi^{in}\rangle$ after it being transformed by the wave plates. Using the retardation wave plates with a fixed optical thickness, one can reconstruct the state varying the orientation of the plates (Fig. 6).

Mathematically one needs to derive a set of equations linking real and imaginary parts of moments (13) and (14) with a coincidence rate. It turns out that the complete set of moments (13) and (14) can be extracted from the projective measurements if two different wave plates are used.

$$|\Psi^{out}\rangle_{kl} = \hat{G}(\delta_1, \theta_k) \hat{G}(\delta_2, \varphi_l) |\Psi^{in}\rangle, \quad (36)$$

where θ_k and φ_l are the orientation angles of the first and second plates. The parameters of the plates, i.e., optical thicknesses for different wavelengths $\delta_{\lambda_j}^{(1,2)}$ and their orientations, are supposed to be known. The projective measurements were carried out by means of a pair of polarization prisms, transmitting the vertical polarization and settled in

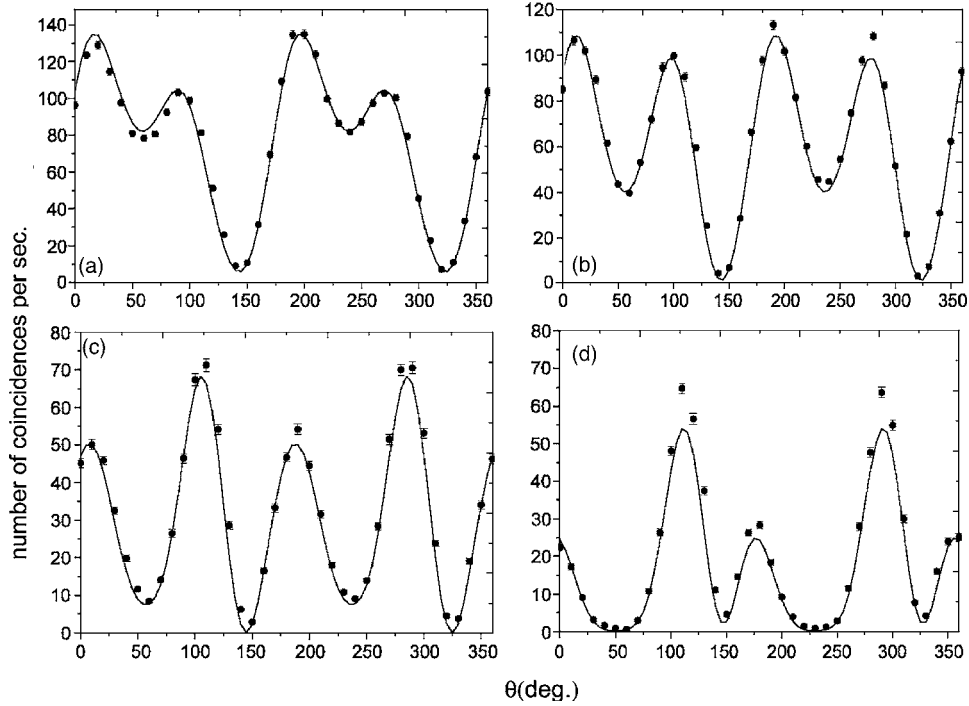
front of each single photon detector in the Brown-Twiss setup. So the number of coincidences is

$$R_{kl} \propto |\langle V_1 V_2 | \Psi^{out} \rangle_{kl}|^2. \quad (37)$$

In order to reconstruct the state it is sufficient to perform at least four measurements corresponding to different orientations of the second plate φ_l and repeat this procedure at least four times varying the orientation of the first plate θ_k . In order to increase the accuracy, we actually performed an excess number of measurements—36 orientations of the second wave plate for each four orientations of the first one. Thus, the total number of measurements μ in this protocol was equal to $4 \times 36 = 144$. Therefore, Protocol 2 includes 148 lines instead of 16 lines used in Protocol 1.

C. Experimental setup

For the generation of biphoton-based ququarts we used lithium-iodate 15 mm crystal pumped with 5 mW cw-helium-cadmium laser operating at 325 nm. The orientation of the crystal was chosen at 58.98° with respect to the pump wave vector. The wavelengths of the collinear down-converted photons were $\lambda_1 = 702$ nm and $\lambda_2 = 605$ nm. For some particular cases we selected biphoton-based ququarts at wavelengths $\lambda_1 = 667$ nm and $\lambda_2 = 635$ nm. Therefore, either $|V_{702}V_{605}\rangle$ or $|V_{667}V_{635}\rangle$ states were used as initial states. Then, these states were subjected to transformations done by dichroic wave plates to prepare a subset of ququarts with $c_1 c_4 = c_2 c_3$ (26). That subset of states was used to be reconstructed. In particular, we used the 0.988 mm (or 0.315 mm) length quartz plate and changed its orientation α , which served as a parameter. Since the thickness of the plate, quartz dispersion and orientation α were supposed to be known, we were able to calculate the result of the state transformation with high accuracy. When Protocol 2 was applied we used the quartz plates with thicknesses 0.821 mm (QP1) and 0.715 mm (QP2). Both protocols were applied to reconstruct the initial state $|\Psi_I(\alpha)\rangle$. In the case when sub-set $c_1 c_4 \neq c_2 c_3$ was generated we used two consecutive 1.8 mm thick type-I BBO (beta-barium borate) crystals with optical axes oriented perpendicularly with respect to each other and at 36.33° with respect to the pump wave vector. An interference filter centered either at 702 nm or at 635 nm and with a full width at half maximum (FWHM) bandwidth of 3 nm was placed in the transmitted arm to make the spectral selection of one photon of the pair, while the photon with conjugated frequency was sent to the reflected arm. As it was already mentioned above, this scheme is equivalent to that one used in [15]. The only difference between our scheme and the one developed in [15] is the following. The scheme described above operates with frequency nondegenerate collinear regime of SPDC instead of noncollinear, frequency degenerate regime used in [15]. Without the loss of generality, this scheme also allows one to reconstruct any arbitrary polarization ququart state by registering the coincidence rate for different projections that are done by the polarization filters located in each arm. Each filter consists of a zero-order quarter- and half-wave plate and a fixed analyzer. Two Si-APD's linked to a coincidence scheme with 1.5 ns time window were used as single photon detectors.

FIG. 7. Dependence of the coincidence rate on tilting angle θ .

D. Results and discussion

We applied both protocols to measure the set of states Ψ_I that were obtained by transforming the initial state $|V_{667\text{ nm}}V_{635\text{ nm}}\rangle$ with quartz plate QP, as it is shown in Fig. 3. We tested the states which were generated for two orientation angles of plate QP $\alpha=0^\circ, 90^\circ$. According to Protocol 2, four sets of measurements were performed for each input state, so totally we performed 148 measurements of the coincidence rate as a function of orientation angles φ_I of QP1 and θ_k of QP2. The dependence of the coincidence rate on the orientation φ_I for $\theta_k=90^\circ$ [Fig. 7(a)], 105° [Fig. 7(b)], 120° [Fig. 7(c)], and 135° [Fig. 7(d)] is shown in Fig. 7. These curves correspond to the measurement of an input state created from $|V_{667\text{ nm}}V_{635\text{ nm}}\rangle$ by QP oriented at $\alpha=20^\circ$ to the vertical direction.

The solid curves give the theoretical behavior of the normalized fourth moment, the dots with bars show the experimental data. Tables II–IV show the results of the statistical reconstruction of ququarts $|\Psi_I\rangle$ performed with the root estimation method. The tables show theoretical and experimental four-dimensional state-vectors $c_{\text{theory}}, c_{\text{exp}}$ as well as fidelity F defined by

$$F = |\langle c_{\text{theory}} | c_{\text{exp}} \rangle|^2. \quad (38)$$

In Table II we present the data measured with Protocol 1 [ququarts with $\lambda_1=702\text{ nm}$ and $\lambda_2=605\text{ nm}$, $h(\text{QP})=0.315\text{ mm}$]. Table III corresponds to measurements performed with Protocol 2 [ququarts with $\lambda_1=667\text{ nm}$ and $\lambda_2=635\text{ nm}$, $h(\text{QP})=0.988\text{ mm}$]. Finally, we demonstrate the validity of preparation, transformation, and measurement procedures performed over biphoton-based ququarts by the reconstruction of Bell states $|\Phi^\pm\rangle$ [$\lambda_1=702\text{ nm}$ and

TABLE II. Results of the state reconstruction measured with Protocol 1. The left column indicates the orientation of the quartz plate QP, determining the state to be measured. The table contains theoretical and experimental state vectors, as well as their fidelities, placed in the right column.

α (deg)	Protocol 1		F
	Theory	Experiment	
0	0	$-0.0295-0.0306i$	0.995
	0	$0.0543-0.0202i$	
	0	$-0.0154-0.0093i$	
	1	0.9972	
10	$-0.0015-0.0229i$	$0.0584-0.1926i$	0.963
	$0.0038-0.0050i$	$0.0073+0.0170i$	
	$0.2013+0.1735i$	$0.1633+0.1233i$	
	0.9638	0.9577	
20	$-0.0021-0.0386i$	$0.0015-0.0326i$	0.976
	$0.0154-0.0162i$	$0.0019-0.0660i$	
	$0.3430+0.3625i$	$0.3967+0.2085i$	
	0.8654	0.8909	
30	$-0.0015-0.0445i$	$-0.0310-0.0542i$	0.991
	$0.0337-0.0225i$	$0.0166-0.0416i$	
	$0.3530+0.5716i$	$0.4526+0.5386i$	
	0.7383	0.7065	
40	$-0.0005-0.0440i$	$0.0112-0.0823i$	0.970
	$0.0511-0.0116i$	$0.1174-0.0328i$	
	$0.1601+0.7466i$	$0.1087+0.8363i$	
	0.6421	0.5167	

TABLE III. Results of the state reconstruction measured with Protocol 2. The left column indicates the orientation of the quartz plate QP, determining the state to be measured. The table contains theoretical, experimental state vectors and their fidelities, placed in the right column.

α (deg)	Protocol 2		F
	Theory	Experiment	
0	0	$-0.0555-0.0204i$	0.996
	0	$-0.0059+0.005i$	
	0	$-0.0425+0.0052i$	
	1	0.9973	
20	0.8097	0.8067	0.998
	$-0.4568-0.3527i$	$-0.4847-0.3304i$	
	$-0.0103-0.0859i$	$0.023-0.0554i$	
	$-0.0316+0.0529i$	$-0.0174+0.0413i$	

$\lambda_2=605$ nm], measured with Protocol 1 and shown in Table IV. As it is seen from the tables, the accuracy of the state reconstruction is a little bit lower when Protocol 1 is applied. It results from the fact that Protocol 1 exploits a minimal number of measurements (16) needed for the four-state system reconstruction. At the same time, since an excess number of measurements (148) was involved when applying the second protocol, the highest accuracy was achieved as in the case of biphoton-based qutrits [12]. The respectively low fidelity for Bell states reconstruction (Table IV) is explained by experimental imperfections at the preparation stage. Preliminary estimation of the prepared state quality can be extracted from visibility that is measured during interference experiments with Bell states. For example, typical visibility observed with space-time interference was 0.9 [26]. Another factor limiting the accuracy of the state reconstruction is the finite number of registered events. In the case of $|\Psi_{II}\rangle$ -set of states we collected about several thousands of coincidences during the accumulation time whereas in the case of $|\Psi_{III}\rangle$ -set only a few hundred coincidences were totally registered.

TABLE IV. Bell states reconstruction. The table contains theoretical, experimental state vectors, and fidelities. The measurements performed with Protocol 1.

Theory	Protocol 1		F
	Experiment		
0.707	0.7326		0.941
0	$0.0818-0.0963i$		
0	$0.0003-0.0281i$		
0.707	$0.6131+0.2657i$		
0.707	0.6597		0.934
0	$0.2518+0.4692i$		
0	$0.0897-0.0319i$		
-0.707	$-0.6155+0.3261i$		

IV. POLARIZATION QUQUARTS IN QKD PROTOCOL

The complete QKD protocol with four-dimensional polarization states exploits five mutually unbiased bases with four states in each [27]. In terms of biphoton states, the first three bases consist of product polarization states of two photons and the last two bases consist of two-photon entangled states:

$$\begin{aligned}
 I. & \quad |H_1H_2\rangle; \quad |H_1V_2\rangle; \quad |V_1H_2\rangle; \quad |V_1V_2\rangle, \\
 II. & \quad |D_1D_2\rangle; \quad |D_1\bar{D}_2\rangle; \quad |\bar{D}_1D_2\rangle; \quad |\bar{D}_1\bar{D}_2\rangle, \\
 III. & \quad |R_1R_2\rangle; \quad |R_1L_2\rangle; \quad |L_1R_2\rangle; \quad |L_1L_2\rangle, \\
 IV. & \quad |R_1H_2\rangle + |L_1V_2\rangle; \quad |R_1H_2\rangle - |L_1V_2\rangle; \\
 & \quad |L_1H_2\rangle + |R_1V_2\rangle; \quad |L_1H_2\rangle - |R_1V_2\rangle, \\
 V. & \quad |H_1R_2\rangle + |V_1L_2\rangle; \quad |H_1R_2\rangle - |V_1L_2\rangle; \\
 & \quad |H_1L_2\rangle + |V_1R_2\rangle; \quad |H_1L_2\rangle - |V_1R_2\rangle. \quad (39)
 \end{aligned}$$

Here $|H\rangle \equiv |1\rangle$, $|V\rangle \equiv |0\rangle$, $|D\rangle \equiv 1/\sqrt{2}(|1\rangle + |0\rangle)$, $\bar{D} \equiv 1/\sqrt{2}(|1\rangle - |0\rangle)$, $|R\rangle \equiv 1/\sqrt{2}(|1\rangle + i|0\rangle)$, $|L\rangle \equiv 1/\sqrt{2}(|1\rangle - i|0\rangle)$ indicate horizontal, vertical, $+45^\circ$ linear, -45° linear, right- and left-circular polarization modes correspondingly. Lower indices numerate the frequency modes of two photons. It has been proved [3] that it is sufficient to use only the first two or three bases for the efficient QKD. When using an incomplete set of bases one sacrifices the security but enhances the keygeneration rate. Since the fulfillment of Bell measurements for the last two bases requires a big experimental effort on both preparation and measurement stages of a protocol, we will restrict ourselves to the first three bases. As we will show experimentally, all states from the first three bases can be prepared with the help of a single nonlinear crystal and local unitary transformations. This is fundamental compared with biphoton-based qutrits, where SU(2) transformations between states from mutually unbiased bases are prohibited. We also present a measurement scheme that allows one to distinguish the states belonging to one basis deterministically thus allowing its implementation in QKD protocol with polarization ququarts.

Experimental procedure

The experimental setup for the generation of ququart states that belong to the first three bases (39) is shown in Fig. 8. To measure a prepared state either Protocol 1 or Protocol 2

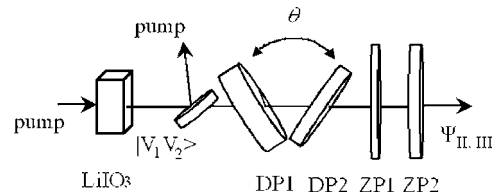


FIG. 8. Setup for preparation and measurement of ququarts which can be used in QKD. Wave plates DP1, DP2 oriented at 45° with respect to the vertical axis serve as the dichroic retardation plate with variable optical thickness which is controlled by tilting angle θ . Two zero-order plates ZP1, ZP2 allow one to choose the basis.

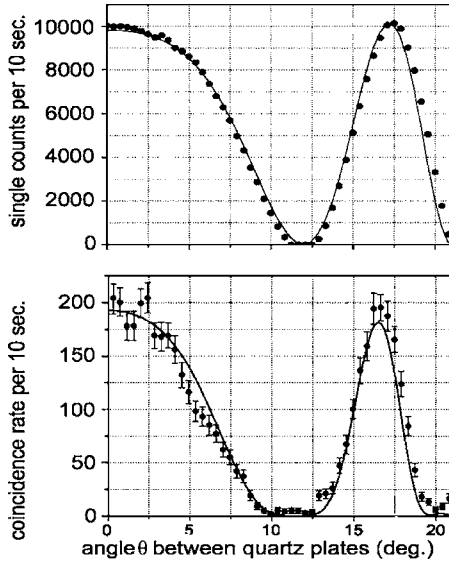


FIG. 9. Dependence of single counts (upper) and coincidences rates (lower) on tilting angle θ .

can be used. Usually we applied Protocol 1 for checking the quartet state.

As an example let us consider the preparation of state $|H_1V_2\rangle$ from initial state $|V_1V_2\rangle$. This transformation can be achieved by a dichroic wave plate that introduces a phase shift of 2π for a vertically polarized photon at 605 nm, a phase shift of π for the conjugated photon. The wave plate is oriented at 45° to the vertical direction. Using quartz plates as retardation material it is easy to calculate that the thickness of the wave plate that does this transformation should be equal to 3.406 mm [28]. Since these wave plates were not readily available and the result of transformation is extremely sensitive to small variations of thickness, we used the following method to achieve the desired thickness. Two quartz plates with geometric thicknesses of 3.716 mm (DP1) and 0.315 mm (DP2) with the orthogonally oriented optical axis were placed consecutively in the biphoton beam. The consecutive action of these two wave plates correspond to the action of the quartz wave plate with an effective thickness of 3.401 mm. If then one can tilt these wave plates towards each other by a finite angle θ , then the optical thickness of the effective wave plate formed by DP1 and DP2 will change, and, at a certain value of θ , the desired transformation will be achieved. This corresponds to the maximal coincidence rate when the measurement part (Protocol 1) is tuned to select state $|H_1V_2\rangle$. Monitoring the coincidences, one can obtain the value of θ for which the maximum occurs. Then, fixing the tilting angle at this value, one can perform a complete quantum state tomography protocol in order to verify if the state really coincides with the ideal. In order to change the basis from I to II (III), zero-order half- (quarter-) wave plates ZP1 (ZP2) oriented at 22.5° (45°) were used. This procedure is repeated for the generation of any of the states. Figure 9 shows the coincidences and single count rates versus the change of tilting angle θ which determines the optical thickness of the effective wave plate. If the measurement setup is tuned to select state $|H_1V_2\rangle$ then the depen-

TABLE V. Fidelities for the states belonging to the first three bases.

I	$ H_1H_2\rangle$	$ H_1V_2\rangle$	$ V_1H_2\rangle$	$ V_1V_2\rangle$
F	0.98	0.94	0.98	0.98
II	$ D_1D_2\rangle$	$ D_1\bar{D}_2\rangle$	$ \bar{D}_1D_2\rangle$	$ \bar{D}_1\bar{D}_2\rangle$
F	0.97	0.96	0.95	0.99
III	$ R_1R_2\rangle$	$ R_1L_2\rangle$	$ L_1R_2\rangle$	$ L_1L_2\rangle$
F	0.95	0.95	0.96	0.97

dence of the coincidence rate on the plate optical thicknesses δ_i is given by the formula:

$$R_{coin} \propto \langle a_1^\dagger b_2^\dagger a_1 b_2 \rangle = \sin^2(\delta_1) \cos^2(\delta_2), \quad (40)$$

whereas the single counts distribution in the upper channel is given by

$$I_{702 \text{ nm}} \propto \langle a_1^\dagger a_1 \rangle = \sin^2(\delta_1), \quad (41)$$

where the optical thickness depends on the tilting angle as follows:

$$\delta_j = \frac{\pi h}{\lambda_j} \left[\frac{(n_e)^2}{\sqrt{(n_e)^2 - \sin^2 \theta}} - \frac{(n_o)^2}{\sqrt{(n_o)^2 - \sin^2 \theta}} \right]. \quad (42)$$

The solid lines in Fig. 9 show the theoretical curves. We performed tomography measurements for both the maxima as well as for the minimum. The minimum in coincidences occurs when intensity in any channel drops to zero, so it is not a necessary condition to distinguish the orthogonal state from that one selected by given settings of polarization filters. Nevertheless according to calculations and our measurements, the minimum in the coincidences in Fig. 9 refers exactly to state $|V_1H_2\rangle$. Starting with $|V_{702 \text{ nm}} V_{605 \text{ nm}}\rangle$, we also prepared and measured the whole set of states from (39) belonging to the first three bases. The result of the state reconstruction is presented in Table V.

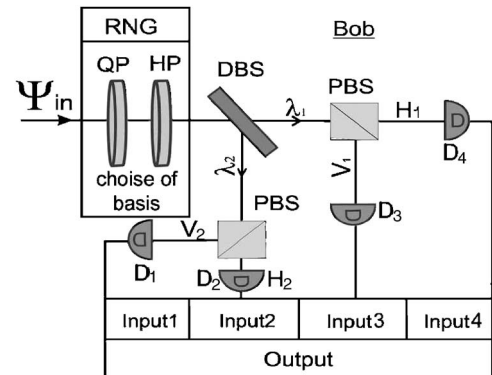


FIG. 10. Measurement part at Bob's station.

TABLE VI. Coincidence rate and density matrix components.

D_4D_2	ρ_{11}	D_4D_1	ρ_{22}	D_3D_2	ρ_{33}	D_3D_1	ρ_{44}
0	0.0(0)	220	0.973(1)	6	0.027(0)	0	0.0(0)

At the same time the method discussed in this section allows one to distinguish unambiguously all states forming chosen bases. The measurement setup that is fulfilling this task and that has been already tested in our experiments is shown in Fig. 10.

It consists of the dichroic mirror, separating the photons with different wavelengths, and a pair of polarization beam-splitters, separating photons with orthogonal polarizations. The four-input double-coincidence scheme linked with the outputs of single-photon detectors registers the biphoton-based ququarts. For example, for the first basis the scheme works as follows, provided that Bob's guess of the basis is correct:

- (i) If state $|H_1H_2\rangle$ comes, then detectors D4, D2 will fire;
- (ii) If state $|H_1V_2\rangle$ comes, then detectors D4, D1 will fire;
- (iii) If state $|V_1H_2\rangle$ comes, then detectors D3, D2 will fire.
- (iv) If state $|V_1V_2\rangle$ comes, then detectors D3, D1 will fire.

The same holds for any of the remaining correctly guessed bases, since the quarter- and half-wave plates transform the polarization into HV basis in which the measurement is performed. The registered coincidence count from a certain pair of detectors contributes to the corresponding diagonal component of the density matrix. So if the basis is guessed correctly, then the registered coincidence count deterministically identifies the input state. We illustrate this statement by Table IV which shows the total number of registered events per 30 s for input state $|R_1L_2\rangle$ measured in the circular basis and calculated components of the experimental (theoretical) density matrix.

The main obstacle for the practical implementation of the free-space QKD protocol based on ququarts is that one needs to perform fast polarization transformation at the selected wavelengths. There are different ways of overcoming this problem and we will discuss them elsewhere. In this section we mention briefly the possible ways. Since it is not practical to tune the tilting wave plates every time one wants to encode a ququart value, we suggest either using a polarization modulator that operates on two wavelengths or splitting the photons with dichroic mirrors and perform these transformations on halves of a biphoton independently in a Mach-Zehnder-like configuration. It is important to note that interferometric accuracy in Mach-Zehnder interferometer is not

needed, since it is used only for spatial separation of photons. The practical solution would be to couple the down-converted photons in a single mode fiber to ensure a perfect spatial mode overlap and then to split them with the wavelength division multiplexer (WDM). Then, the switching between the states can be done with the polarization modulators that introduce a π or 2π phase shifts for the selected wavelength. The choice of basis on Alice's side is performed by zero-order quarter- and half-wave plates, which can be realized within the Pockel (Liquid Crystal) cell driven by a randomly selected voltage. Free space communication is proposed since it is not practical to distribute a polarization state within an optical fiber. On Bob's side, the random choice of basis [random number generator (RNG)] is performed in the same way as on Alice's side. Then photons are spatially separated with the help of WDM or a dichroic mirror and each of the photons is sent to the Brown-Twiss scheme with a polarizing beam-splitter that projects an arrived photon on a H or V state as it is shown in Fig. 10. Moreover, registering coincidences allows one to circumvent the problem of the detection noise that is common for single photon based protocols. If the coincidence window is quite small, it is possible to assure a lower level of accidental coincidences for the usual dark count rate of single photon detectors (Table VI).

In conclusion, we have suggested and tested a method of preparation and measurement of subset of four-dimensional polarization quantum states. Since for this class of states the polarization degree is not invariant under $SU(2)$ transformations, it is possible to switch between orthogonal states using linear transformations (namely geometrical rotations and phase shifts).

Note added. Recently, we learned about closely related work performed by R. B. R. Adamson and co-authors [29].

ACKNOWLEDGMENTS

Stimulating discussions with G. Björk and V. P. Karassiov are gratefully acknowledged. This work was supported in part by the Russian Foundation of Basic Research (Project Nos. 05-02-16391a, 06-02-16769, 06-02-16393a) and the Leading Russian Scientific Schools (Project No. 4586.2006.2). S.P.K. acknowledges support from the Russian Ministry of Science and Education (Project Nos. 2006-RI-19.0/001/593 and 2-435/2005).

- [1] D. Kaszlikowski, P. Gnacinski, M. Zukowski, W. Miklaszewski, and A. Zeilinger, *Phys. Rev. Lett.* **85**, 4418 (2000); D. Kaszlikowski, D. K. L. Oi, M. Christandl, K. Chang, A. Ekert, L. C. Kwek, and C. H. Oh, *Phys. Rev. A* **67**, 012310 (2003); T. Durt, N. J. Cerf, N. Gisin, and M. Zukowski, *ibid.* **67**, 012311 (2003); D. Collins, N. Gisin, N. Linden, S. Massar, and S. Popescu, *Phys. Rev. Lett.* **88**, 040404 (2002).
- [2] H. Bechmann-Pasquinucci and A. Peres, *Phys. Rev. Lett.* **85**, 3313 (2000); D. Bruß and C. Macchiavello, *ibid.* **88**, 127901 (2002); **88**, 127901 (2002); D. Horoshko and S. Kilin, *Opt. Spectrosc.* **94**, 691 (2003).
- [3] H. Bechmann-Pasquinucci and W. Tittel, *Phys. Rev. A* **61**, 062308 (2000); M. Bourennane, A. Karlsson, and G. Björk, *ibid.* **64**, 012306 (2001); N. J. Cerf, M. Bourennane, A. Karlsson, and N. Gisin, *Phys. Rev. Lett.* **88**, 127902 (2002); F. Caruso, H. Bechmann-Pasquinucci, and C. Macchiavello, *Phys. Rev. A* **72**, 032340 (2005).
- [4] S. Walborn, D. Lemelle, M. Almeida, and P. Ribeiro, *Phys. Rev. Lett.* **96**, 090501 (2006).
- [5] S. Gröblacher, T. Jennewein, A. Vaziri, G. Weihs, and A. Zeilinger, *New J. Phys.* **8**, 75 (2006).
- [6] M. O’Sullivan-Hale, I. Ali Khan, R. Boyd, and J. Howell, *Phys. Rev. Lett.* **94**, 220501 (2005); L. Neves, G. Lima, J. G. Aguirre Gomez, C. H. Monken, C. Saavedra, and S. Padua, *ibid.* **94**, 100501 (2005).
- [7] A. Vaziri, G. Weihs, and A. Zeilinger, *Phys. Rev. Lett.* **89**, 240401 (2002); A. Vaziri, J.-W. Pan, T. Jennewein, G. Weihs, and A. Zeilinger, *ibid.* **91**, 227902 (2003); N. K. Langford, R. B. Dalton, M. D. Harvey, J. L. O’Brien, G. J. Pryde, A. Gilchrist, S. D. Bartlett, and A. G. White, *ibid.* **93**, 053601 (2004).
- [8] H. de Riedmatten, I. Marcikic, V. Scarani, W. Tittel, H. Zbinden, and N. Gisin, *Phys. Rev. A* **69**, 050304(R) (2004).
- [9] R. T. Thew, A. Acín, H. Zbinden, and N. Gisin, *Quantum Inf. Comput.* **4**(2), 93 (2004); R. T. Thew, A. Acín, H. Zbinden, and N. Gisin, *Phys. Rev. Lett.* **93**, 010503 (2004).
- [10] J. C. Howell, A. Lamas-Linares, and D. Bouwmeester, *Phys. Rev. Lett.* **88**, 030401 (2002).
- [11] Yu. Bogdanov, M. Chekhova, S. P. Kulik, G. Maslennikov, M. K. Tey, and C. Ch. Oh, *Phys. Rev. Lett.* **93**, 230503 (2004).
- [12] Yu. Bogdanov, M. Chekhova, L. Krivitsky, S. P. Kulik, L. C. Kwek, M. K. Tey, C. Ch. Oh, and A. A. Zhukov, *Phys. Rev. A* **70**, 042303(R) (2004).
- [13] D. N. Klyshko, *Photons and Nonlinear Optics* (Gordon and Breach, New York, 1988).
- [14] A. V. Belinsky and D. N. Klyshko, *Laser Phys.* **4**, 663 (1994).
- [15] D. F. V. James, P. G. Kwiat, W. J. Munro, and A. G. White, *Phys. Rev. A* **64**, 052312 (2001).
- [16] A. V. Burlakov and M. V. Chekhova, *JETP Lett.* **75**, 432 (2002).
- [17] M. V. Chekhova, L. A. Krivitsky, S. P. Kulik, and G. A. Maslennikov, *Phys. Rev. A* **70**, 053801 (2004).
- [18] V. P. Karassiov, *J. Phys. A* **26**, 4345 (1993).
- [19] G. Björk, J. Söderholm, A. Trifonov, P. Usachev, L. L. Sanchez-Soto, and A. V. Klimov, *Proc. SPIE* **4750**, 1 (2002); A. Sehat, J. Soderholm, G. Björk, P. Espinoza, A. B. Klimov, and L-L. Sanchez-Soto, *Phys. Rev. A* **71**, 033818 (2005).
- [20] D. N. Klyshko, *JETP* **84**, 1065 (1997).
- [21] Of course, it is possible to chose specific orthogonal qutrit states that might be transformed into each other by geometrical rotations and phase shifts. These states are: $|HV\rangle$, $|RL\rangle$, and $|D\bar{D}\rangle$. According to our definition these states possess $P=0$ whereas its unit polarization degree is introduced in [19]. The concept of biphoton-based qutrits orthogonality and their transformation properties are discussed in detail in [17].
- [22] A. V. Burlakov, S. P. Kulik, Yu. Rytikov, and M. V. Chekhova, *JETP* **95**, 639 (2002).
- [23] L. Mandel and E. Wolf, *Optical Coherence and Quantum Optics* (Cambridge University Press, Cambridge, MA, 1995).
- [24] Y. H. Kim, S. P. Kulik, and Y. Shih, *Phys. Rev. A* **63**, 060301(R) (2001).
- [25] Yu. I. Bogdanov, R. F. Galeev, S. P. Kulik, G. A. Maslennikov, and E. V. Moreva, *JETP Lett.* **82**, 164 (2005).
- [26] When studying “space-time” interference for polarization-type entangled states (27) the dependence of coincidence rate on phase delay φ_{14} is analyzed by setting the polarization filters at $\pm 45^\circ$.
- [27] Bases are mutually unbiased if the inner products between all possible pairs of vectors belonging to different bases have the same magnitude equal to $1/\sqrt{D}$, where D is the dimension of the Hilbert space.
- [28] The thickness of the retardation plate that performs the transformation is determined by the number of order m_i that is chosen for the specified wavelength according to $m_1\lambda_1/\delta n_1=(2m_2+1)\lambda_2/2\delta n_2$. Here δn_i is the value of the birefringence for the specific wavelength. We chose order $m_1=51$ for $\lambda=702$ nm and $m_2=47$ for $\lambda=650.2$ nm.
- [29] R. B. A. Adamson, L. K. Shalm, M. W. Mitchell, and A. M. Steinberg, e-print quant-ph/0601134.